μ-Spec Spectrometers for the EXCLAIM Instrument

Mona Mirzaei[a,b], Emily M. Barrentine[a], Berhanu T. Bulcha[a], Giuseppe Cataldo[a], Jake A. Connors[d], Negar Ehsan[a], Thomas M. Essinger-Hileman[a], Larry A. Hess[a], Jonas W. Mugge-Durum[a,e], Omid Noroozian[a], Trevor M. Oxholm[a,f], Thomas R. Stevenson[a], Eric R. Switzer[a], Carolyn G. Volpert[a,e], and Edward J. Wollack[a]

[a]NASA Goddard Space Flight Center, Greenbelt, MD, USA
[b]Science Systems and Applications, Inc., Lanham, MD, USA
[c]University of Maryland, Baltimore County, MD, USA
[d]National Institute of Standards and Technology, Boulder, CO, USA
[e]University of Maryland, College Park, MD, United States
[f]University of Wisconsin, Madison, WI, United States

ABSTRACT

The EXperiment for Cryogenic Large-aperture Intensity Mapping (EXCLAIM) is a cryogenic balloon-borne instrument that will map carbon monoxide and singly-ionized carbon emission lines across redshifts from 0 to 3.5, using an intensity mapping approach. EXCLAIM will broaden our understanding of these elemental and molecular gases, and the role they play in star formation processes across cosmic time scales. The focal plane of EXCLAIM's cryogenic telescope features six μ-Spec spectrometers. μ-Spec is a compact, integrated grating-analog spectrometer, which uses meandered superconducting niobium microstrip transmission lines on a single-crystal silicon dielectric to synthesize the grating. It features superconducting aluminum microwave kinetic inductance detectors (MKIDs), also in a microstrip architecture. The spectrometers for EXCLAIM couple to the telescope optics via a hybrid planar antenna coupled to a silicon lenslet. The spectrometers operate from $420-540\,\mathrm{GHz}$ with a resolving power $R = \lambda/\Delta\lambda = 512$, and employ an array of 355 MKIDs on each spectrometer. The spectrometer design targets a noise equivalent power (NEP) of $2 \times 10^{-18}\,\mathrm{W}/\sqrt{\mathrm{Hz}}$ (defined at the input to the main lobe of the spectrometer lenslet beam, within a 9° half width), enabled by the cryogenic telescope environment, the sensitive MKID detectors, and the low dielectric loss of single-crystal silicon. We report on these spectrometers under development for EXCLAIM, providing an overview of the spectrometer and component designs, the spectrometer fabrication process, fabrication developments since previous prototype demonstrations, and the current status of their development for the EXCLAIM mission.

Keywords: sub-millimeter astronomy, integrated spectrometer, superconducting transmission line, microwave kinetic inductance detector

1. INTRODUCTION

Multiwavelength imaging observations have revealed a wide range of environments in the universe.[1] In the past 40 years, utilizing far-infrared and submillimeter spectroscopy, galaxies at redshifts as large as $z = 7.5$ have been confirmed with space and ground-based facilities.[2] These, and related optical observations, indicate an increase in the star formation rate from the cosmological reionization period up until redshifts of $z = 2$.[1,3,4] After reaching this peak, the star formation rate falls by a factor of 10. To obtain a better understanding of the evolution of the physical conditions of galaxies across cosmic time, and how these influence the star formation rate, new measurements of the molecular and fine-structure emission lines of abundant elements such as carbon, nitrogen and oxygen are needed.

Corresponding authors:
M.M: E-mail: mona.mirzaei@nasa.gov
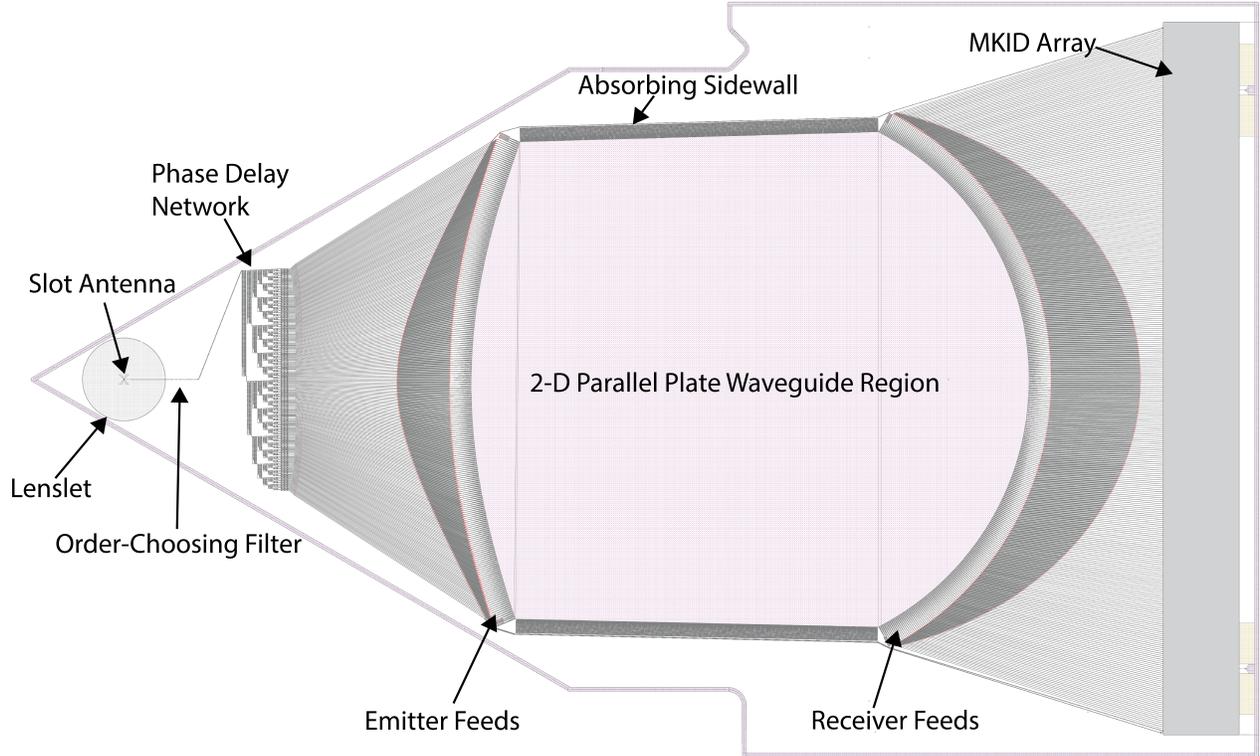E.M.B.: E-mail: emily.m.barrentine@nasa.gov

Figure 1: The EXCLAIM μ-Spec spectrometer design. The spectrometer chip is 34 mm × 59 mm in size.

The EXperiment for Cryogenic Large-Aperture Intensity Mapping (EXCLAIM)[5,6] is a new high-altitude balloon spectrometer mission that is designed to detect the submillimeter emission of redshifted carbon monoxide (CO) and singly-ionized carbon [CII] lines in windows spanning $0 < z < 3.5$. Instead of resolving individual galaxies and measuring their brightness, EXCLAIM will measure the statistics of brightness fluctuations of redshifted, cumulative line emission, in a method known as intensity mapping (IM). It will provide a blind and complete survey of the emitting gas in a cross-correlation with the Baryon Oscillation Spectroscopic Survey (BOSS).[7] IM reduces aperture and integration requirements relative to surveys that catalog individual galaxies, allowing the science goals to be achieved in a conventional balloon flight. The optimal band for BOSS cross correlation is $420 - 600$ GHz; however, a bright ortho-water emission line in the upper atmosphere occurs at 557 Hz. To avoid that emission,[3] EXCLAIM operates from $420 - 540$ GHz.

EXCLAIM fields six μ-Spec spectrometers on an all-cryogenic (1.7 K) telescope. μ-Spec[8–11] integrates all the elements of a grating spectrometer onto a silicon chip, which due to the high index of silicon, provides an order of magnitude reduction in size compared to designs that employ a free space grating. We report here on the status of the μ-Spec spectrometers under development for EXCLAIM, including the EXCLAIM spectrometer and component designs, expected performance, fabrication development and the planned spectrometer fabrication process.

2. THE EXCLAIM μ-SPEC DESIGN

The EXCLAIM μ-Spec design operates from $420 - 540$ GHz, with a resolving power of $R = \lambda/\Delta\lambda \sim 512$, and an expected noise-equivalent power NEP of 2×10^{-18} W/$\sqrt{\text{Hz}}$, defined at the input to the main lobe of the spectrometer lenslet beam (within a 9° half width), when under the typical expected sky loading in the primary science channels (0.7 fW at the spectrometer lenslet input, assuming an optical efficiency of 74%

Table 1: The EXCLAIM μ-Spec spectrometer and MKID design parameters.

Number of spectrometers	6
Spectrometer spectral band	$420 - 540\,\text{GHz}$
Spectrometer grating order, M	2 (single order)
Spectrometer resolving power, R	512 at 472 GHz (center frequency)
	$535 - 505$ over spectral band
Spectrometer efficiency	23%
Spectrometer NEP (at input to lenslet main lobe)	$2 \times 10^{-18}\,\text{W}/\sqrt{\text{Hz}}$ at 0.70 fW (typical loading)
MKID NEP (at input to each MKID)	$5 \times 10^{-19}\,\text{W}/\sqrt{\text{Hz}}$ at 0.16 fW (typical loading)
Number of receivers/MKIDs per spectrometer	355
MKID readout band	$3.25 - 3.75\,\text{GHz}$
Operating temperature	100 mK

through the telescope optics). A schematic of the EXCLAIM μ-Spec design is shown in Figure 1, and a summary of the EXCLAIM μ-Spec design and performance parameters are listed in Table 1. The integrated μ-Spec spectrometer design is realized in niobium planar transmission line on a thin (450 nm thick), and low-loss[12–15] single-crystal silicon dielectric, and is based on the μ-Spec design approach previously demonstrated as an $R = 64$ prototype.[10,11]

Light is coupled to the spectrometer from the optics of the EXCLAIM telescope via an on-chip planar slot antenna with a silicon lenslet. The slot antenna design is based on a cross-slot design approach,[16] and operates over a full octave ($300 - 600\,\text{GHz}$). The slot antenna is located at the focus of a 4 mm diameter hyper-hemispherical silicon lenslet, which is attached to the back of the spectrometer silicon chip. A parylene-C anti-reflection (AR) coating is applied to the spherical surface of the silicon lenslet, with a thickness optimized to provide optimal coupling over the EXCLAIM band. Further details of the EXCLAIM optics design are provided in Ref. 17 in these proceedings.

An impedance-transforming microstripline feed couples to the slot antenna and transmits the signal to the microstripline phase delay network. Here the signal is split in N=256 branches, in a binary tree configuration using broadband ($300 - 600$ GHz) 4-stage Wilkinson power dividers. A linear phase delay gradient is applied by adjusting the length of meandered microstripline in this power splitting network. The resulting phase-delayed wavefronts are then launched via emitter feeds into a 2D parallel-plate waveguide, and recombine constructively at receiver feeds located at angles along the spectrometer focal plane as a function of wavelength, in a Rowland circle configuration[18,19] with a Rowland circle radius of 1.35 cm. These receiver feeds Nyquist sample the sinc^2 spectral function of the synthesized grating. The focal plane receiver and emitter locations and the transmission line lengths of the phase delay network are optimized[20] taking into account dispersion effects due to the kinetic inductance of the niobium planar transmission line and due to the geometry and bends of the meandered delay network. The length of the microstrip line between the power splitters in the binary tree network is also designed to avoid the occurrence of stopbands in the EXCLAIM band due to coherent reflections off of the bends.[8] In addition, the angles of the receivers are constrained to viewing angles of $\leq 45\%$ with respect to the emitter array to optimize coupling. This focal plane and delay network design spans a single grating order, $M = 2$, provides diffraction-limited phase error over the spectrometer band, amd spectral resolving power of $R = NM = 512$ at the center frequency of the EXCLAIM spectral band. The order of the spectrometer grating is selected by an on-chip stepped-impedance microstripline "order-choosing" bandpass filter with a passband from $345 - 603$ GHz located at the input of the spectrometer phase delay network, by low- and high-pass metal-mesh filters inserted in the EXCLAIM telescope optics, and by the niobium transmission lines, which terminate light above the superconducting energy gap at ∼680 GHz.

Each receiver feed transitions back to microstrip and to an individual MKID detector. There are 355 receivers and MKIDs on each spectrometer and all of the MKIDs on a spectrometer are read out on a single 50 Ohm aluminum microstrip microwave feedline, with the MKIDs coupled via a parallel-plate coupling capacitor formed between the top aluminum layer and an isolated region of the niobium ground plane layer. The MKIDs consist
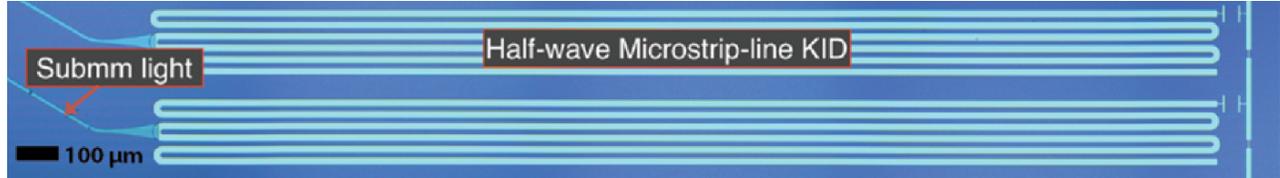
Figure 2: An aluminum half-wave microstrip transmission line design will be employed for the MKIDs in the EXCLAIM µ-Spec design, similar to the design used for the $R = 64$ µ-Spec prototype MKID array, which is shown above.

of two branches of a half-wave microstrip transmission-line resonator, with a 20-nm-thick aluminum microstrip absorbing layer and a niobium ground plane. Their resonance frequencies span $3.25 - 3.75$ GHz. The sub-millimeter optical input lies at the microwave zero voltage node, between two branches of symmetric half-wave transmission line resonators, providing isolation between the microwave and sub-millimeter optical signals. This EXCLAIM MKID design is similar to the one shown in Figure 2, which was used in the $R = 64$ µ-Spec demonstration, but features a thinner and narrower aluminum microstripline for increased sensitivity. The spectrometer and MKIDs operate at 100 mK bath temperature. Aluminum MKIDs have demonstrated excellent sensitivity with NEPs as low as $\sim 10^{-19}$ W/$\sqrt{\text{Hz}}$.[21] Based upon our measurements of microwave loss, two-level system (TLS) noise and quasiparticle heating effects in representative ~ 20 nm thick aluminum coplaner waveguide (CPW) resonators structures (similar to the niobium CPW resonator structures described in Section 4) our design models predicts an MKID NEP of $\sim 5 \times 10^{-19}$ W/$\sqrt{\text{Hz}}$, under the typical expected loading in the primary science channels (0.16 fW at the input to each MKID).

The expected efficiency of the spectrometer from the input of the lenslet to the input of each MKID is estimated to be $\sim 23\%$. Sources of loss include the optical coupling of the slot-antenna lenslet beam to the EXCLAIM receiver optics (estimated loss of 51%), loss in the coupling between the receiver and emitter feeds in the spectrometer focal plane (estimated loss of 50%, due to limitations of the chosen feed design), and loss in the planar transmission lines dominated by loss in the silicon dielectric (estimated loss of $\leq 5\%$).

The geometry of the microstrip transmission line provides high immunity to stray light and cross-talk, due to the thin 450-nm-thick silicon dielectric layer and the protective niobium ground plane. In the 2D parallel plate waveguide cavity a meta-material absorbing sidewall structure[22] provides $\geq 99\%$ attenuation of signals over a full octave ($300 - 600$ GHz) and over a range of incidence angles (45-90 degrees). This sidewall absorber structure provides additional termination for any out-of-band signals, and of any reflections in the 2D waveguide cavity. In addition, a thin film titanium absorber with sheet resistance ~ 150 Ohms/square is deposited on the back of the spectrometer silicon chip to limit the coupling of stray power to the detectors through the silicon. Thermal blocking filters[23] can be added at the input to the microwave readout lines of the spectrometer package. The spectrometer focal plane package design also features a baffle structure to reduce the field of view, and absorbing sidewalls, to attenuate stray light before it reaches the sensitive detectors.

3. SPECTROMETER FABRICATION

The EXCLAIM µ-Spec fabrication follows a process similar to that used for the $R = 64$ prototypes devices, though new developments to the process will be discussed in Section 4. In this process, superconducting aluminum and niobium films are patterned on both sides of the single-crystal silicon device layer of a silicon-on-insulator (SOI) wafer, using a low-temperature flip-bonding process.[24] The process begins with an SOI wafer with a float-zone (f-z) silicon device layer of 450 nm thickness for the dielectric. The niobium ground plane layer is fabricated via a lift off process (similar to that described in Refs. 24, 25) to avoid roughening and etching through the silicon device layer. The niobium lift-off process is performed using germanium as a hard mask. This process starts by applying hexamethyldisilazane (HMDS) and a thin layer of photoresist ($0.5 - 1\,\mu$m) followed by a soft bake to remove the solvent. A thin layer of germanium is then deposited via evaporation or sputtering. This germanium layer is masked by another layer of HMDS and photoresist, which are baked at low temperature over a long duration and are exposed via a contact mask. The lower temperature of the bake protects the germanium from

thermal shock and the long time is needed to remove all the solvents in the resist. Then the germanium is etched with Reactive Ion Etching (RIE). The photoresist is then ashed in an O_2 plasma to remove the top layer and define the undercut in the lift-off profile. The niobium ground plane is deposited via sputtering, while the silicon native oxide is etched just prior to deposition. In the final step, the niobium pattern is lifted-off by acetone.

A benzocyclobutene (BCB) polymer resin is used to bond the niobium ground plane side of the SOI wafer to the front side of the f-z silicon wafer. The SOI handle wafer is removed by a combination of lapping and etching. The buried oxide layer is removed with a Buffered Oxide Etch (BOE) to expose the other side of the silicon device layer. A similar lift-off process with a germanium hard mask is then used to define the top niobium microstrip circuitry while preventing damage to the silicon dielectric layer. For this top-side niobium patterning, a two-step lithography process using a contact mask and direct writing, is performed. The direct write is used to obtain the sub-micron feature sizes required for the slot antenna feed design. A gold-palladium (AuPd) layer (sheet resistance of ~ 20 Ohms/square) with a titanium (Ti) adhesion layer is then deposited between, and over, regions of the niobium microstrip lines using a resist lift-off mask. This Ti/AuPd layer forms the absorber in the spectrometer focal plane sidewalls, and in the power dividers in the phase delay network. The next step in the process is to pattern the aluminum layer which forms the MKID array structure. To ensure the proper aluminum film profile and a clean silicon interface, the native oxide on the silicon is removed by a hydrogen fluoride (HF) dip and a reverse bias clean is completed just prior to the aluminum deposition (see further details of this process in Section 4). After sputter-depositing the aluminum, HMDS and a thin resist layer are applied for the lithography. The photoresist is patterned via either a contact mask or a combination of contact mask and direct writing, followed by a gentle develop step. Protected by the resist, the aluminum is wet etched in aluminum etchant and the remaining resists are stripped in solvent.

In the next step, the device layer is etched to provide access to the ground plane niobium for wirebonding purposes. Then a protective resist is applied to protect the wafer frontside and the titanium resistive layer is deposited on the back side of the supporting silicon backing wafer. The titanium is etched back by BOE, while it is masked by the photoresist. In the last step, the final release of the wafer is performed in acetone. This full process is illustrated in Figure 3.

4. FABRICATION DEVELOPMENT

A two-layer lift-off process was developed[24] for the $R = 64$ μ-Spec prototype to pattern the thin film super-conducting niobium microstrip transmission lines (as described in Section 3) and resulted in a US patent.[26] This original technique provided the precise control of linewidth ($\leq \pm 0.2\,\mu$m) required to ensure phase control in the microstrip transmission lines and thus the high resolution of the spectrometer. However, results of the initial prototype $R = 64$ μ-Spec spectrometers, and separate diagnostic CPW resonator devices, showed that unexpected loss was being introduced due to the lift-off process. This extra loss was determined to be due to thin extended sidewalls of the niobium, at the edge of the niobium traces, resulting from the sputter-deposited lift-off process (Figure 5a), and an amorphous native oxide layer at the niobium-silicon substrate interface (Figure 4a).

An improved lift-off technique using a two-step selective etching method was developed to provide a clean metal-silicon interface and to remove the lossy extended sidewalls. In this modified lift-off process, the amorphous native oxide layer on the silicon substrate is removed by either a BOE or a reverse bias cleaning process, just prior to the deposition of the niobium film (Figure 4b). After the lift-off is complete, a self-limited layer of niobium oxide is grown on the surface and subsequently removed by wet etching to remove the thin extended tails. The oxidation-wet etch step is repeated for as many cycles as necessary (Figure 5b). In developing this modified lift-off process, niobium CPW quarter-wave resonators with a "fishbone" resonance frequency tuning structure[27] (Figure 6) were used for a rapid turn-around study of the impacts of process variations on internal microwave quality factors, Q_i. Coupling quality factor, Q_c, values for these diagnostic resonators ranged from $\sim 5{,}000$ to $\sim 500{,}000$ and resonance frequencies were at ~ 3.5 GHz. The CPW readout feedline in these devices was formed from the same niobium layer and there were no subsequent fabrication steps. These CPW devices were tested at base temperatures of $7 - 30$ mK, inside a magnetically-shielded and light-tight dilution refrigerator. Table 2 reports the microwave loss of four individual devices, with or without sidewall removal and pre-cleaning of the native oxide. For comparison purposes, measurements for etched niobium resonator samples, previously
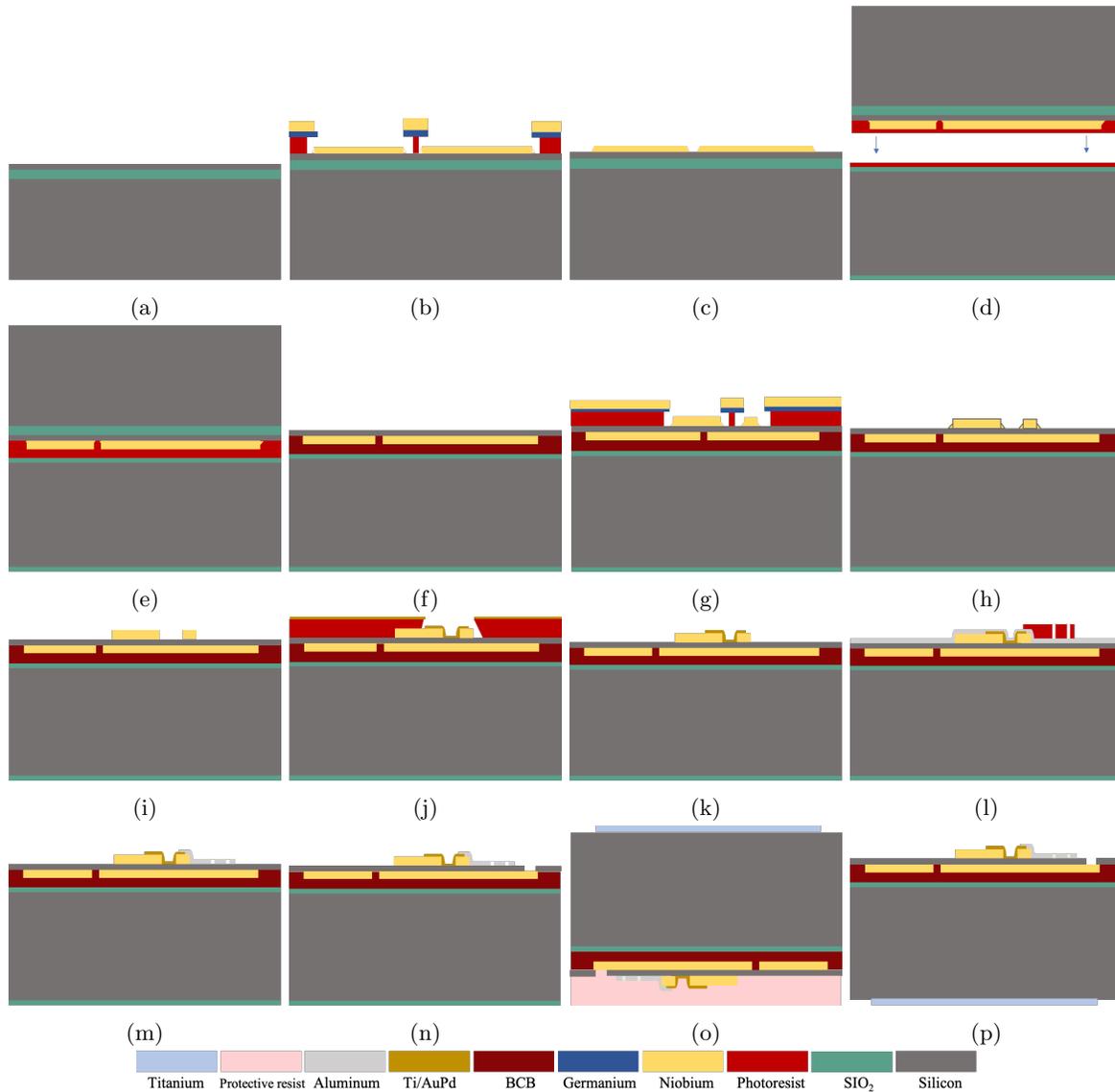
Figure 3: The planned spectrometer fabrication process flow. a) Begin with an SOI wafer. b) A photo-resist/germanium hard mask is patterned. The germanium is etched by RIE. Then masked by the germanium, the resist underlayer is ashed in an O_2 plasma to remove the resist layer and define the mask undercut. The niobium ground layer is deposited via sputtering. The silicon (Si) native oxide is etched just prior to deposition. c) The lift-off process is completed to define the niobium ground plane layer. d) and e) The niobium ground plane side of the wafer is bonded to a fz-silicon backing wafer coated with thermal oxide using a BCB polymer resin. f) The SOI handle wafer is removed by a combination of lapping and etching. The SOI buried oxide layer is removed with BOE. g) A photo-resist/germanium hard mask for the top-side niobium circuitry is patterned. The germanium hard mask is etched by RIE. Masked by the germanium, the resist underlayer is ashed in an O_2 plasma to remove the top layer and define the undercut. The top niobium layer is sputtered-deposited through the mask, with removal of the native oxide layer just prior to deposition. h) The top niobium lift-off is completed. Then a self-limited layer of niobium oxide is grown on the surface and subsequently removed by wet etching. i) This oxidation-wet etch cycle is repeated as necessary to remove the extended sidewalls. j) A lift-off resist mask is patterned and the Ti/AuPd absorber layer is deposited. k) The Ti/AuPd layer is lifted off. l) After sputter-depositing the aluminum, the photoresist is applied and patterned. m) The aluminum layer is wet etched. n) The SOI silicon device layer is etched through for access to the ground plane. o) The wafer frontside is protected by resist and the backside thermal oxide on the silicon backing wafer is removed, followed by patterning of the titanium absorber layer. p) The spectrometer wafer is released in acetone.

reported in Ref. 28, are also shown. The modified lift-off process results in a decrease in microwave loss by more than an order of magnitude when measured in these CPW microwave resonator structures.
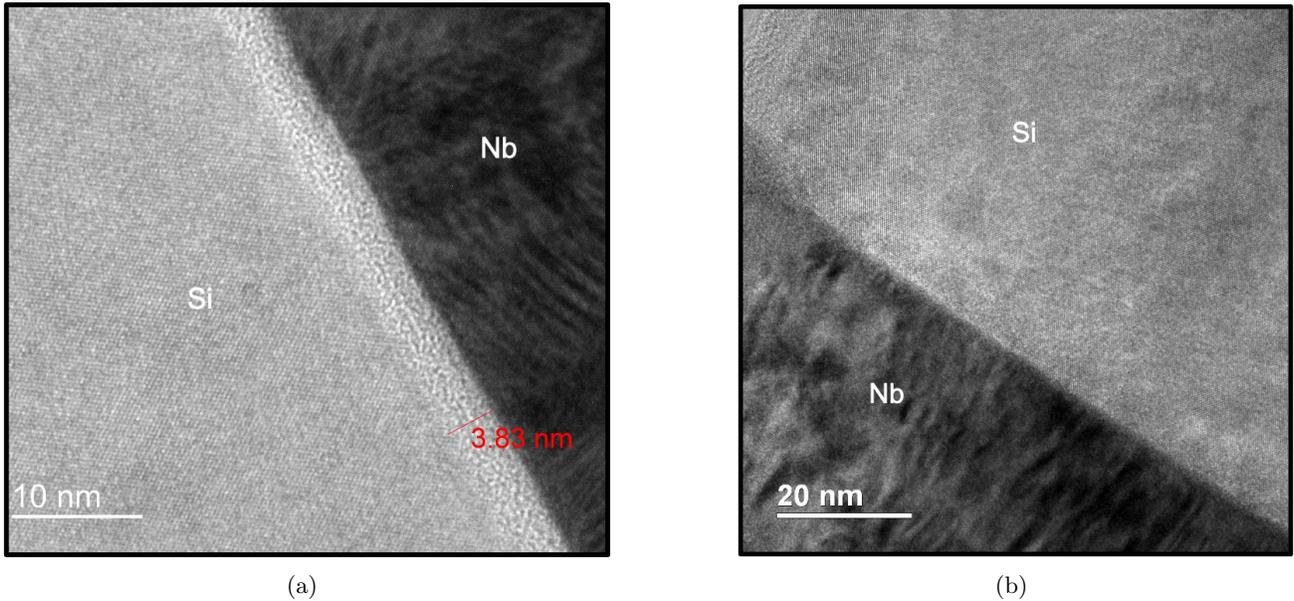

<table>
<tr><td>(a)</td><td>(b)</td></tr>
</table>

Figure 4: a) Transmission electron microscopy (TEM) image showing the ground plane niobium (Nb)-silicon (Si) interface of an $R = 64$ μ-Spec prototype. Here there is evidence of an amorphous layer which was a source of TLS loss. b) TEM image showing the Nb-Si interface of a CPW resonator, which underwent a modified niobium lift-off process with a BOE clean of the native oxide prior to the niobium deposition and removal of the extended sidewalls. Here the contact is sharp, with no evidence of amorphous layers.

The EXCLAIM MKID arrays employ a 20 nm thick aluminum layer, with narrower linewidths than were required for the aluminum MKID arrays in the $R = 64$ prototype. In the design of the microstrip transmission line for the resonators, the coupling capacitor structures and the microstrip feedline, aluminum linewidths of ∼0.8 to 1.7 μm were originally considered, though the design has since converged to minimum linewidths of ∼1.3 μm. To fabricate these features with precise control on the width variation and to protect the thin single-crystal silicon dielectric from roughening and etching, contact and high-resolution direct laser writing lithography patterning steps, followed by a wet aluminum etch process, have been developed. These processes need to ensure contact between the spectrometer sub-millimeter niobium transmission lines and the aluminum MKID structure. Proper step coverage and surface cleaning is important to obtain a low resistance electrical contact and low microwave loss. To control the etch rate of the aluminum for sub-micron-to-micron feature sizes, the aluminum etch is performed at room temperature, which reduces the etch rate to 40 Å/sec compared to the nominal etch rate of 125 Å/sec at 50 C. Figure 7 shows scanning electron microscope (SEM) images of the silicon surface after the aluminum wet etch process. Initially, evidence of residual aluminum (which could lead to TLS noise and loss) was seen after the completion of the etch. Additional substrate cleaning with a reverse bias prior to the aluminum deposition was found to be a critical step to address this issue.

5. CURRENT STATUS

Fabrication of the EXCLAIM μ-Spec spectrometers began in October 2020 and will follow the processes described in Sections 3 and 4. Characterization of the resulting individual spectrometers and their MKID arrays, including measurement of the NEP, resolving power, and absolute frequency response of the spectrometer channels is planned prior to their integration into the EXCLAIM receiver and instrument. The first EXCLAIM balloon flight is anticipated in late summer or fall 2022.
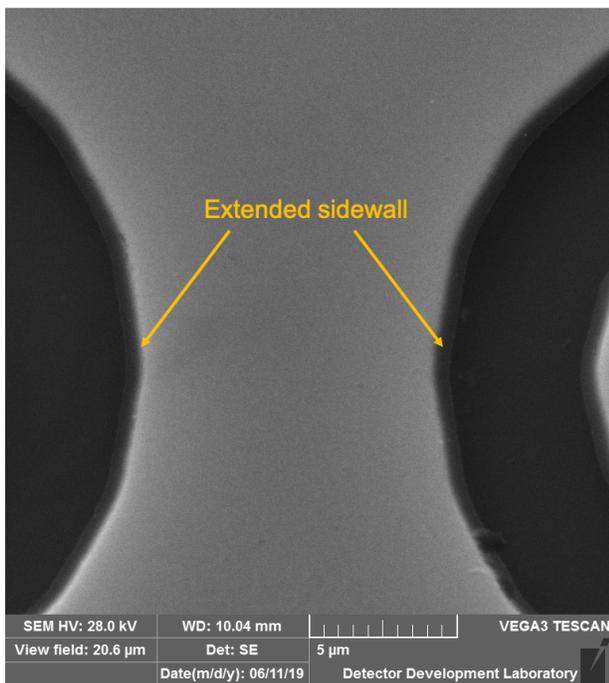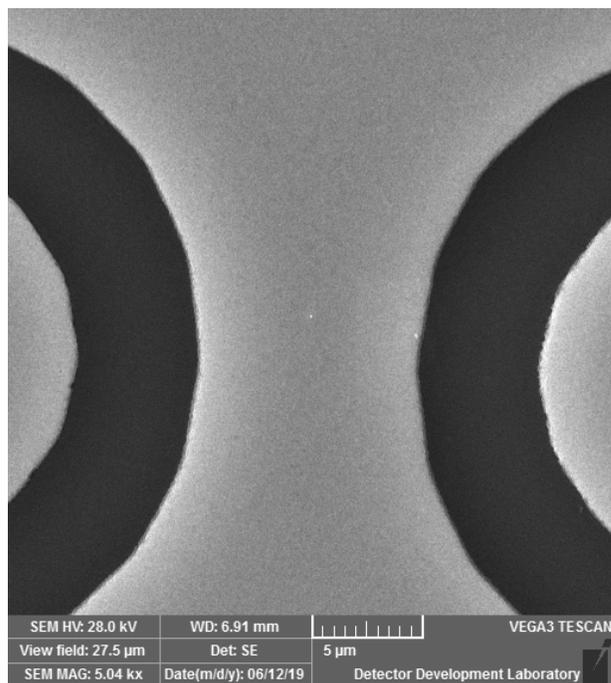
(a)   (b)

Figure 5: a) SEM image of the as deposited niobium lift-off pattern. Note the thin extended sidewalls at the edges of the pattern, which have been observed to result in higher microwave loss and low Q_i in CPW resonator structures. b) After successive oxidation and etch cycles the extended sidewalls are removed and the resulting measured Q_i is more than $10\times$ higher (see Table 2).
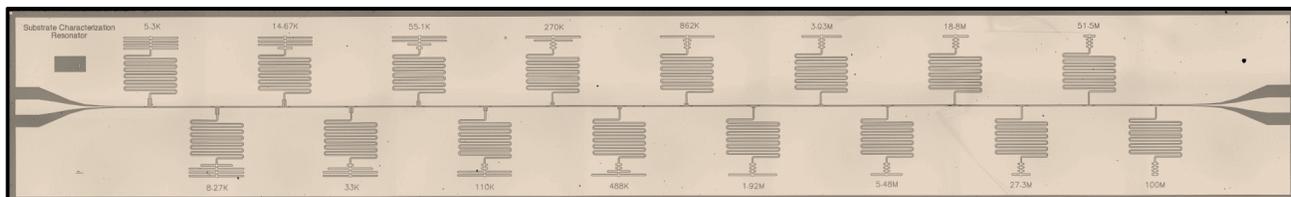

Figure 6: Image of a niobium CPW resonator chip, featuring quarter-wave resonators with "fishbone" tuning structures. This resonator chip design was used as a diagnostic device, to measure microwave loss in response to variations in the niobium lift-off process.

Table 2: Comparison table of microwave loss and residual resistivity ratio (RRR) measurements for niobium CPW resonators chips with modifications to the niobium lift-off process. Also included for comparison are etched niobium devices. All devices measured were CPW resonators with a fishbone tuning structures (see Figure 6).

Primary Process Differences	Microwave Q_i Readout power $= -130$ dBm	Microwave Q_i Readout power $= -80$ dBm	Film RRR
* Reactive ion etch of Nb	400,000-1,000,000	200,000-400,000	5.9
* Nb lift-off * BOE clean prior to deposition * Removal of sidewalls	200,000	100,000-150,000	5.7
* Nb lift-off * Reverse bias prior to deposition * Removal of sidewalls	150,000-350,000	100,000-200,000	5.0
* Nb lift-off * BOE clean prior to deposition * No removal of sidewalls	10,000-20,000	7,000-10,000	7.0
* Nb lift-off * No native oxide removal * No removal of sidewalls	4,000-8,000	4,000-8,000	6.3

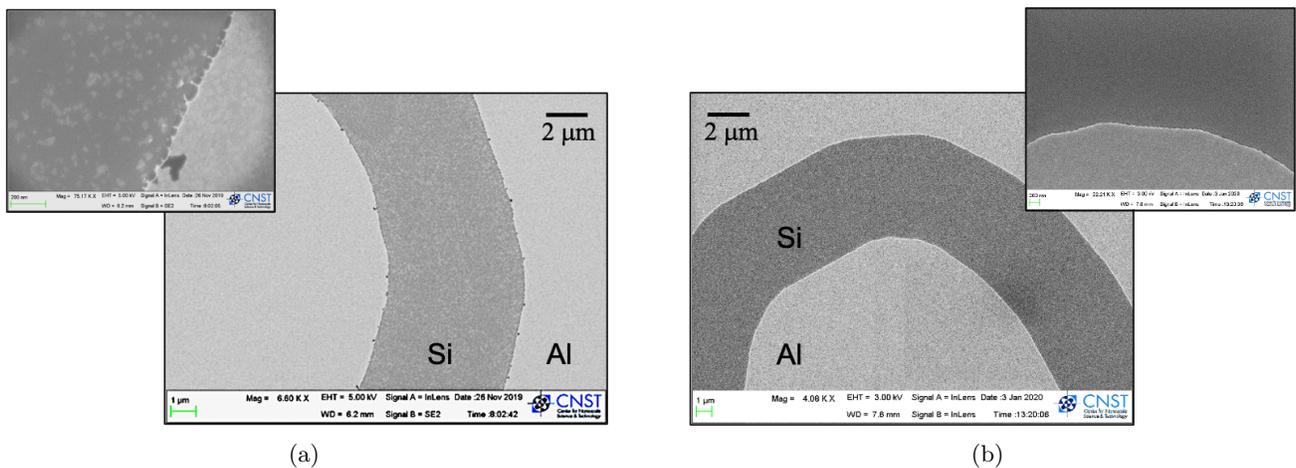(a)   (b)

Figure 7: a) SEM image of a wet-etched aluminum layer on silicon. Note the residual aluminum in the etched regions in the absence of cleaning prior to the deposition. b) Applying a reverse bias prior to the aluminum deposition improves the quality of the etch and clears the residual aluminum in the etched area.

ACKNOWLEDGMENTS

REFERENCES

[1] P. Madau, M. D., "Cosmic star-formation history," *Annu. Rev. Astron. Astrophys.* **52**, 415–486 (2014).

[2] S. L. Finkelstein, e. a., "A galaxy rapidly forming stars 700 million years after the big bang at redshift 7.51," *Annu. Rev. Astron. Astrophys.* **502**, 524–527 (2013).

[3] C. Carilli, F. W., "Cool gas in high-redshift galaxies," *Annu. Rev. Astron. Astrophys.* **51**, 105–161 (2013).

[4] Walter, F., Carilli, C., Neeleman, M., Decarli, R., Popping, G., Somerville, R. S., Aravena, M., Bertoldi, F., Boogaard, L., Cox, P., et al., "The evolution of the baryons associated with galaxies averaged over cosmic time and space," *The Astrophysical Journal* **902**(2), 111 (2020).

[5] Ade, P., Anderson, C., Barrentine, E., Bellis, N., Bolatto, A., Breysse, P., Bulcha, B., Cataldo, G., Connors, J., Cursey, P., et al., "The experiment for cryogenic large-aperture intensity mapping (EXCLAIM)," *Journal of Low Temperature Physics* , 1–11 (2020).

[6] Cataldo, G. et al., "Design and performance of a high resolution μ-Spec: an integrated sub-millimeter spectrometer," in [*Millimeter, Submillimeter, and Far-Infrared Detectors and Instrumentation for Astronomy X*], International Society for Optics and Photonics (2020).

[7] Alam, S., Albareti, F. D., Prieto, C. A., Anders, F., Anderson, S. F., Anderton, T., Andrews, B. H., Armengaud, E., Aubourg, É., Bailey, S., et al., "The eleventh and twelfth data releases of the sloan digital sky survey: final data from SDSS-III," *The Astrophysical Journal Supplement Series* **219**(1), 12 (2015).

[8] Barrentine, E. M., Cataldo, G., Brown, A. D., Ehsan, N., Noroozian, O., Stevenson, T. R., Kongpop, U.-Y., Wollack, E. J., and Moseley, S. H., "Design and performance of a high resolution μ-Spec: an integrated sub-millimeter spectrometer," in [*Millimeter, Submillimeter, and Far-Infrared Detectors and Instrumentation for Astronomy VIII*], **9914**, 99143O, International Society for Optics and Photonics (2016).

[9] Cataldo, G., Moseley, S. H., and Wollack, E. J., "A four-pole power-combiner design for far-infrared and submillimeter spectroscopy," *Acta Astronautica* **114**, 54–59 (2015).

[10] Cataldo, G., Hsieh, W.-T., Huang, W.-C., Moseley, S. H., Stevenson, T. R., and Wollack, E. J., "Microspec: an ultracompact, high-sensitivity spectrometer for far-infrared and submillimeter astronomy," *Applied optics* **53**(6), 1094–1102 (2014).

[11] Noroozian, O., Barrentine, E., Brown, A., Cataldo, G., Ehsan, N., Hsieh, W.-T., Stevenson, T., U-yen, K., Wollack, E., and Moseley, S. H., "μ-spec: An efficient compact integrated spectrometer for submillimeter astrophysics," in [*26th International Symposium on Space Terahertz Technology*], (2015).

[12] Datta, R., Munson, C., Niemack, M., McMahon, J., Britton, J., Wollack, E. J., Beall, J., Devlin, M., Fowler, J., Gallardo, P., et al., "Large-aperture wide-bandwidth antireflection-coated silicon lenses for millimeter wavelengths," *Applied optics* **52**(36), 8747–8758 (2013).

[13] Loewenstein, E. V., Smith, D. R., and Morgan, R. L., "Optical constants of far infrared materials. 2: Crystalline solids," *Applied optics* **12**(2), 398–406 (1973).

[14] Afsar, M. N. and Chi, H., "Millimeter wave complex refractive index, complex dielectric permittivity and loss tangent of extra high purity and compensated silicon," *International Journal of Infrared and Millimeter Waves* **15**(7), 1181–1188 (1994).

[15] Wollack, E. J., Cataldo, G., Miller, K. H., and Quijada, M. A., "Infrared properties of high-purity silicon," *Optics Letters* **45**(17), 4935–4938 (2020).

[16] Iacono, A., Freni, A., Neto, A., and Gerini, G., "In-line x-slot element focal plane array of kinetic inductance detectors," in [*Proceedings of the 5th European Conference on Antennas and Propagation (EUCAP)*], 3316–3320, IEEE (2011).

[17] Essinger-Hileman, T. et al., "Optical design of the experiment for cryogenic large-aperture intensity mapping (EXCLAIM)," in [*Millimeter, Submillimeter, and Far-Infrared Detectors and Instrumentation for Astronomy X*], International Society for Optics and Photonics (2020).

[18] Rotman, W. and Turner, R., "Wide-angle microwave lens for line source applications," *IEEE Transactions on antennas and propagation* **11**(6), 623–632 (1963).

[19] Rowland, H. A., "XXIX. on concave gratings for optical purposes," *The London, Edinburgh, and Dublin Philosophical Magazine and Journal of Science* **16**(99), 197–210 (1883).

[20] Giuseppe Cataldoa, E. M. B., Berhanu T. Bulchaa, Negar Ehsan, L. A. H., Omid Noroozian, T. R. S., Edward J. Wollack, S. H. M., and Switzer, E. R., "Second-generation Micro-Spec: A compact spectrometer for far-infrared and submillimeter space missions," *Acta Astronautica* **162**, 155–157 (2019).

[21] Baselmans, J. J., Bueno, J., Yates, S. J., Yurduseven, O., Llombart, N., Karatsu, K., Baryshev, A., Ferrari, L., Endo, A., Thoen, D., et al., "A kilo-pixel imaging system for future space based far-infrared observatories using microwave kinetic inductance detectors," *Astronomy & Astrophysics* **601**, A89 (2017).

[22] Bulcha, B., Cataldo, G., Stevenson, T., U-Yen, K., Moseley, S., and Wollack, E., "Electromagnetic design of a magnetically coupled spatial power combiner," *Journal of Low Temperature Physics* **193**(5-6), 777–785 (2018).

[23] Wollack, E., Chuss, D., Rostem, K., and U-Yen, K., "Impedance matched absorptive thermal blocking filters," *Review of Scientific Instruments* **85**(3), 034702 (2014).

[24] Patel, A., Brown, A.-D., Hsieh, W.-T., Stevenson, T., Moseley, S. H., Kongpop, U., Ehsan, N., Barrentine, E., Manos, G., Wollack, E. J., et al., "Fabrication of MKIDS for the MicroSpec spectrometer," *IEEE transactions on applied superconductivity* **23**(3), 2400404–2400404 (2013).

[25] Brown, A.-D., Brekosky, R., Franz, D., Hsieh, W.-T., Kutyrev, A., Mikula, V., Miller, T., Moseley, S. H., Oxborrow, J., Rostem, K., et al., "Fabrication of ultrasensitive TES bolometric detectors for HIRMES," *Journal of Low Temperature Physics* **193**(5-6), 675–680 (2018).

[26] Brown, A. D. and Patel, A. A., "High precision metal thin film liftoff technique," (July 7 2015). US Patent 9,076,658.

[27] Stevenson, T. R., Adams, J. S., Hsieh, W.-T., Moseley, S. H., Travers, D. E., Kongpop, U., Wollack, E. J., Zmuidzinas, J., et al., "Superconducting films for absorber-coupled mkid detectors for sub-millimeter and far-infrared astronomy," *IEEE transactions on applied superconductivity* **19**(3), 561–564 (2009).

[28] Brown, A. D., Barrentine, E. M., Moseley, S. H., Noroozian, O., and Stevenson, T., "The impact of standard semiconductor fabrication processes on polycrystalline Nb thin-film surfaces," *IEEE Transactions on Applied Superconductivity* **27**(4), 1–5 (2016).